Prostate Cancer: Prediction of Biochemical Failure after External-Beam Radiation Therapy—Kattan Nomogram and Endorectal MR Imaging Estimation of Tumor Volume[1]

Antonio C. Westphalen, MD
Walter J. Koff, MD
Fergus V. Coakley, MD
Valdair F. Muglia, MD
John M. Neuhaus, PhD
Ralph T. Marcus, MD
John Kurhanewicz, PhD
Rebecca Smith-Bindman, MD

Purpose: To determine whether magnetic resonance (MR) imaging and MR spectroscopic imaging findings can improve predictions made with the Kattan nomogram for radiation therapy.

Materials and Methods: The institutional review board approved this retrospective HIPAA-compliant study. Ninety-nine men who underwent endorectal MR and MR spectroscopy before external-beam radiation therapy for prostate cancer (January 1998 to June 2007) were included. Linear predictors were calculated with input variables from the study sample and the Kattan original coefficients. The linear predictor is a single weighted value that combines information of all predictor variables in a model, where the weight of each value is its association with the outcome. Two radiologists independently reviewed all MR images to determine extent of disease; a third independent reader resolved discrepancies. Biochemical failure was defined as a serum prostate-specific antigen level of 2 ng/mL (2 μg/L) or more above nadir. Cox proportional hazard models were used to determine the probabilities of treatment failure (biochemical failure) in 5 years. One model included only the Kattan nomogram data; the other also incorporated imaging findings. The discrimination performance of all models was determined with receiver operating characteristics (ROC) curve analyses. These analyses were followed by an assessment of net risk reclassification.

Results: The areas under the ROC curve for the Kattan nomogram and the model incorporating MR imaging findings were 61.1% (95% confidence interval: 58.1%, 64.0%) and 78.0% (95% confidence interval: 75.7%, 80.4%), respectively. Comparison of performance showed that the model with imaging findings performed significantly better than did the model with clinical variables alone ($P < .001$). Overall, the addition of imaging findings led to an improvement in risk classification of about 28%, ranging from approximately a minimum of 16% to a maximum of 39%, depending on the risk change considered important.

Conclusion: MR imaging data improve the prediction of biochemical failure with the Kattan nomogram after external-beam radiation therapy for prostate cancer. The number needed to image to improve the prediction of biochemical failure in one patient ranged from three to six.

[1] From the Department of Radiology and Biomedical Imaging (A.C.W., F.V.C., J.K., R.S.) and Epidemiology and Biostatistics (J.M.N.), University of California San Francisco, 505 Parnassus Ave, Box 0628, Room M-372, San Francisco, CA 94143-0628; Department of Urology, Federal University of Rio Grande do Sul, Porto Alegre, Rio Grande do Sul, Brazil (W.J.K.); Department of Radiology, Riberão Preto School of Medicine, University of São Paulo, Riberão Preto, São Paulo, Brazil (V.F.M.); Department of Radiology, Tufts Medical Center, Boston, Mass (R.T.M.); and Department of Radiology, UCSF-Mt Zion Medical Center, San Francisco, Calif (R.S.).
Received March 1, 2011; revision requested April 21; final revision received May 10; accepted May 19; final version accepted June 10. **Address correspondence to** A.C.W. (e-mail: *antoniocarlos.westphalen@ucsf.edu*).

Currently, an estimated 30% of patients select external-beam radiation therapy as their primary mode of treatment for prostate cancer (1–3). Yet, despite our best efforts in selecting appropriate therapy, up to 50% of these patients, depending on risk factors, will develop biochemical failure within 5 years, leaving room for improvement (1–3). Prostate cancer treatment options are numerous, and accurate prediction of patient outcome is an increasingly important guide for appropriate treatment of the disease. Men in whom there is an increased likelihood of failure of routine treatment protocols may receive tailored therapies. On the contrary, men in whom treatment is unlikely to fail will have more confidence to proceed to prescribed therapies.

The development of nomograms and risk classifications represents an advance in prediction efforts. These charts or diagrams are built on the basis of a statistical model, and the model is designed to predict the outcome of individual patients and help both patients and physicians with decision making, particularly which treatments are more desirable. The nomograms and risk classifications combine multiple known risk factors, usually pretreatment clinical variables such as prostate-specific antigen (PSA) level, clinical stage, and biopsy Gleason score, to determine the risk of posttreatment recurrence and/or to predict the histopathologic stage of the cancer (4). The Kattan nomogram for radiation therapy (5,6) is a widely used and accepted method. It uses a combination of five variables that are entered into the equation—baseline PSA level, clinical stage, Gleason score, radiation dose, and use of androgen deprivation therapy—and is intended to calculate the progression-free probability after external-beam radiation therapy. Progression refers to biochemical failure (increasing PSA level after a nadir has been reached). The likelihood of biochemical failure is at least in part dependent on the presence of micrometastasis at the time of local therapy, and, although the adequate length of treatment is still a matter of debate, prior studies have shown that the combination of androgen deprivation therapy with local treatment leads to decreased rates of treatment failure (7,8). The Kattan nomogram can, therefore, be seen as a tool that estimates the probability of underlying microscopic metastatic disease prior to therapy. The most recent version of the nomogram was built on the basis of posttreatment outcome of over 2000 patients from the Memorial Sloan-Kettering Cancer Center (New York, NY) (6). The input for each one of the variables that are part of the nomogram is associated with a certain number of points, and the total number of points is associated with a certain progression-free probability (Fig 1). The risk of failure is the complement of the progression-free probability.

Unfortunately, despite incorporating variables that have been shown to be good predictors of treatment outcome, these nomograms have had limited success (4). In part, this is a result of inherent limitations of the variables incorporated in these models. The Gleason score, for instance, is based on biopsy results, but biopsy has known problems. With biopsy, just a small fraction of the gland is sampled, and even extensive biopsy protocols do not depict up to 30% of cancers (9–11), particularly those localized in the apex and anterior parts of the prostate (12), many of which represent large, high-grade cancers. Similarly, and also because of sampling errors, the Gleason score of tumors may be underestimated (13,14). Likewise, pretreatment PSA level may reflect, at least to a certain extent, the presence of benign prostatic hyperplasia (15). The generalization of a certain nomogram is also limited by variations in clinical practice and subtle differences in radiation therapy planning and execution.

In addition, the variables that are part of these prediction tools (16,17) provide limited anatomic and no metabolic information. Such data could improve outcome predictability and offer additional information to allow for the development of individualized treatment protocols. Endorectal magnetic resonance (MR) imaging has emerged as an accurate method of evaluating the aggressiveness and extent of prostate cancer (18–26). Previous publications have demonstrated that MR imaging and/or MR spectroscopic imaging findings are predictive of radiation treatment outcome, particularly in intermediate and high-risk groups (27–31). Wang et al (32,33) have shown that the addition of endorectal MR imaging and MR spectroscopic imaging to staging nomograms results in added value in predicting organ-confined prostate cancer in patients before radical prostatectomy. The extent

Advance in Knowledge

- MR imaging and MR spectroscopic imaging findings can improve the predictions of biochemical failure following external-beam radiation therapy made with the Kattan nomogram for radiation therapy.

Implication for Patient Care

- One in every three to six patients who undergo MR imaging prior to treatment may benefit from improved prediction of response to radiation therapy.

Published online before print
10.1148/radiol.11110457 **Content code:** GU

Radiology 2011; 261:477–486

Abbreviations:
IQR = interquartile range
PSA = prostate-specific antigen
ROC = receiver operating characteristic
SD = standard deviation

Author contributions:
Guarantors of integrity of entire study, A.C.W., R.T.M.; study concepts/study design or data acquisition or data analysis/interpretation, all authors; manuscript drafting or manuscript revision for important intellectual content, all authors; approval of final version of submitted manuscript, all authors; literature research, A.C.W., R.T.M.; clinical studies, A.C.W., V.F.M., R.T.M., J.K.; experimental studies, R.T.M.; statistical analysis, J.M.N., R.T.M., R.S.; and manuscript editing, A.C.W., W.J.K., V.F.M., J.M.N., R.T.M., J.K., R.S.

Funding:
This research was supported by the National Institutes of Health (grant KL2 RR024130).

Potential conflicts of interest are listed at the end of this article.

of disease affects treatment planning; because many patients who elect radiation therapy rather than radical prostatectomy have more aggressive and higher volume of disease, examination of this population is particularly suited to efforts to improve staging nomograms.

Accordingly, our goal was to determine whether MR imaging and MR spectroscopic imaging findings can improve the predictions made with the Kattan nomogram for radiation therapy.

Materials and Methods

Subjects

Our Committee on Human Research approved this Health Insurance Portability and Accountability Act–compliant retrospective cohort study. We searched all hospital information systems to identify patients who underwent endorectal MR and MR spectroscopy prior to external-beam radiation therapy for prostate cancer from January 1998 to June 2007. One hundred ten patients were identified, of whom nine were excluded because of lack of any follow-up and two were excluded because images were not interpretable because of artifacts from an endovascular stent and a hip prosthesis. The final group consisted of 99 men (Fig 2).

Kattan Nomogram

The Kattan nomogram calculates the patient's probability of progression-free survival after external-beam radiation therapy for prostate cancer. The inputs to the nomogram are serum PSA level, clinical stage that is based on digital rectal examination findings, sum of Gleason grades, use of neoadjuvant androgen deprivation therapy, and radiation dose (Fig 1) (5,6). We obtained the coefficients of the Kattan nomogram (6), which allowed us to calculate the linear predictors by using the input variables from our sample. Thus, we were able to calculate failure probabilities on the basis of the original nomogram.

Imaging Technique

MR studies were performed with a 1.5-T whole-body MR imaging unit (Signa; GE Medical Systems, Milwaukee, Wis). Ninety-five patients were examined by using the body coil for excitation and a pelvic phased array coil (GE Medical Systems) in combination with a commercially available balloon-covered expandable endorectal coil (Medrad, Pittsburgh, Pa) for signal reception. The balloon was inflated with air (n = 76) or perfluorohydrocarbon (3M, St Paul, Minn) (n = 23). Four patients were imaged by using the same

Figure 1

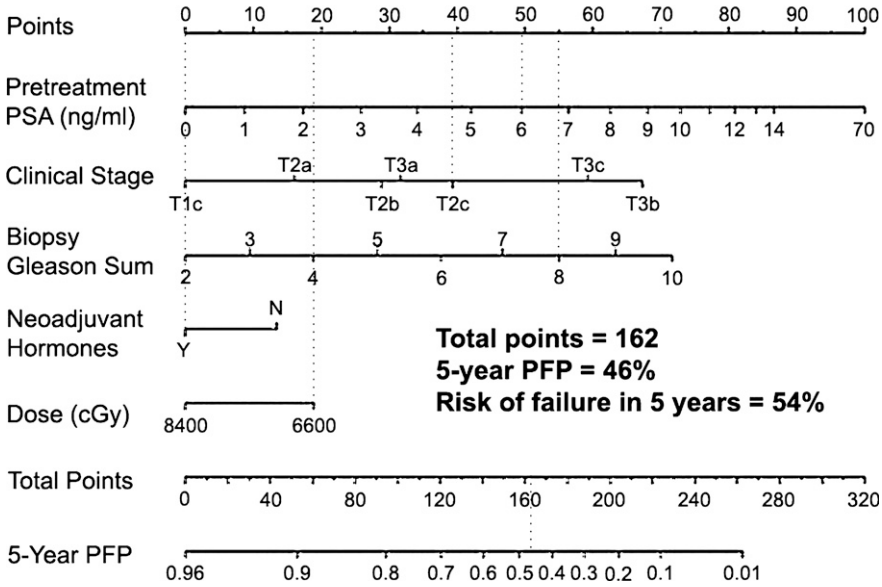

Figure 1: Kattan nomogram for predicting freedom from PSA failure, defined as nadir plus 2 ng/mL (2 μg/L), after three-dimensional conformal radiation therapy and intensity-modulated radiation therapy. In this example, a hypothetical patient who presents with a pretreatment PSA of 6 ng/mL (6 μg/L) (49 points), clinical stage T2c (39 points), and Gleason score 8 (55 points) and who undergoes neoadjuvant therapy (0 points) followed by low-dose radiation (19 points) would have a 46% chance of not having PSA failure in 5 years or, conversely, a 54% chance of having failed treatment (total points, 162). To convert PSA level in nanograms per milliliter to micrograms per liter, multiply by 1.0. *N* = no, *PFP* = progression-free probability, *Y* = yes. (Reprinted and adapted, with permission, from reference 6.)

Figure 2

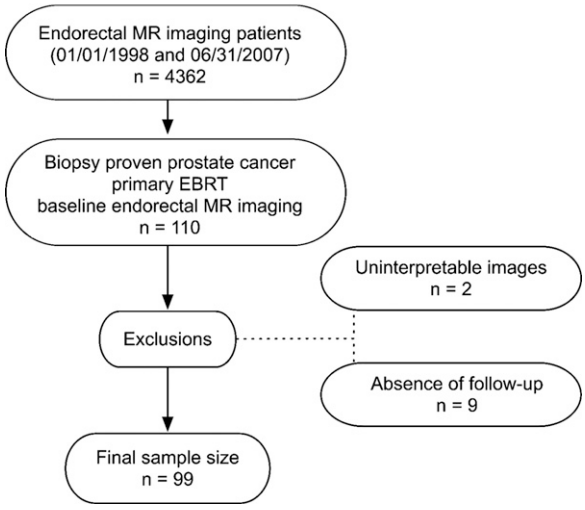

Figure 2: Flowchart of patient selection. *EBRT* = external-beam radiation therapy.

Figure 3

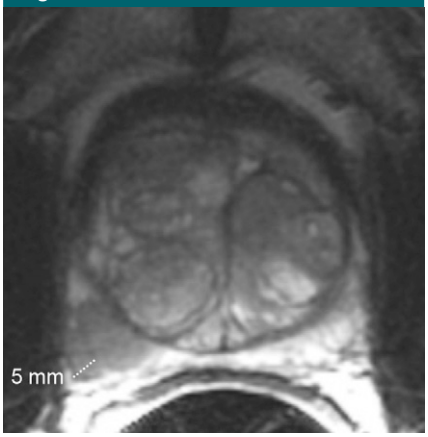

Figure 3: Clinical stage T2a, Gleason 4+3 prostate cancer and benign prostatic hyperplasia in 65-year-old man. Axial T2-weighted MR image (5000/96) shows 5 mm of extracapsular extension in the right posterior part of the midgland.

technique, but with a rigid coil (USA Instruments, Aurora, Ohio). MR imaging included acquisition of thin-section high-spatial-resolution axial and coronal T2-weighted fast spin-echo images of the prostate and seminal vesicles with the following parameters: Repetition time msec/echo time msec (effective), 4876–6550/90–105; echo train length, 16; section thickness, 3 mm; intersection gap, 0 mm; field of view, 14–17 cm; matrix, 256 × 192; and number of signals acquired, three. Anteroposterior frequency encoding was used to prevent obscuration of the prostate by endorectal coil motion artifact.

After review of the axial T2-weighted images, a volume of prostate tissue was selected under the supervision of one of the authors (J.K., with 20 years of experience) to maximize coverage of the gland without including the adjacent rectum and periprostatic fat. Three-dimensional spectroscopic data were acquired by using a water- and lipid-suppressed double spin-echo point-resolved spectroscopic sequence that used spectral-spatial pulses for the two 180° excitation pulses, optimized for quantitative detection of choline, creatine, and citrate. The spectral spatial pulses allowed for both sharp volume selection and frequency selection to reduce water resonance and suppress lipid resonance. The influence of chemical shift on the apparent location of the selected volume was also reduced by the higher spectral bandwidth of the spectral-spatial pulses (34,35). Outer voxel saturation pulses were also used to further sharpen volume selection and conform the selected volume to the shape of the prostate to eliminate susceptibility artifacts from periprostatic fat and rectal air (36). Data sets were acquired as 16 × 8 × 8 phase-encoded spectral arrays, with the following parameters: 1000/130 and a 17-minute acquisition time.

Three-dimensional MR spectroscopic imaging data were processed off-line at a workstation (UltraSparc; Sun Microsystems, Mountain View, Calif) with use of software previously developed specifically for three-dimensional MR spectroscopic imaging studies. All spectral data were apodized with a 2-Hz Lorentzian function and were Fourier transformed in the time domain and in three spatial domains with phase, baseline, and frequency corrections. Integrated peak area values for choline, creatine, and citrate and peak area ratios of choline to creatine and choline plus creatine to citrate were automatically calculated for each voxel. MR spectroscopic imaging data, including spectra and associated metabolic ratios, were overlaid on the corresponding transverse T2-weighted images.

Imaging Interpretation

Two radiologists (F.V.C. and V.F.M., with 14 and 7 years of experience, respectively) independently reviewed all images at a picture archiving and communication system workstation (Impax; Agfa, Mortsel, Belgium). The readers knew that the patients had biopsy-proved prostate cancer and subsequently were treated with radiation therapy, but they were unaware of any other clinical and histopathologic findings, including patient outcome.

Imaging criteria for analysis listed below were selected on the basis of results of previous literature that have shown that the proposed variables are associated with tumor volume, tumor extent, and treatment failure (27,30,37,38).

MR imaging.—The number of sextants with visible tumor on MR images was counted. A sextant was considered positive if a focal masslike nodule or crescentic subcapsular focus of low T2 signal intensity was identified.

Extracapsular extension was considered present if tumor abutted the prostate capsule and demonstrated an irregular margin with the adjacent periprostatic tissue, or if frank extension of tumor outside the confines of the prostatic capsule was present. When seen, extracapsular extension was quantified by measuring (in millimeters) the largest radial (linear) diameter of extraprostatic tumor, defined as the perpendicular distance of tumor beyond the expected location of the outer capsular margin (Fig 3).

The presence or absence of seminal vesicle invasion was noted. Seminal vesicle invasion was considered present if a low-signal-intensity tumor on T2-weighted images was seen, indicating enlargement and/or loss of normal seminal vesicle architecture, irrespective of side or number of seminal vesicles involved.

MR spectroscopic imaging.—The number of sextants demonstrating malignant voxels on MR spectroscopic images was counted. Unequivocal malignant metabolism was defined as elevation of the choline peak and/or reduction of the citrate peak, leading to a spectrum in which the choline peak is clearly greater than the citrate peak. This pattern has been shown to be strongly associated with malignancy (38).

A third reader (A.C.W., with 6 years of experience) independently adjudicated all disagreements, and the adjudicated data were used for the analysis.

Diagnosis, Patient Treatment, and Outcome

One of the authors performed a thorough review of medical charts to determine the details of patients' diagnosis, treatment, and outcome. The following data were extracted: age, pretreatment PSA level, clinical stage, Gleason score, date of radiation treatment, treatment dose, use of hormonal therapy, PSA level nadir, date of biochemical failure

(if appropriate), PSA level at the time of biochemical failure, and date of patient's last PSA level. *Biochemical failure* was defined as an increase in serum PSA level of 2 ng/mL (2 μg/L) or more above the nadir PSA level (39,40).

Statistical Analysis

Descriptive statistics of mean and median (and measures of dispersion) were used to summarize the patient cohort with respect to clinical, imaging, and outcome variables.

Cox proportional hazard models for multiple predictors were used to determine the probabilities of treatment failure (biochemical failure) in 5 years. The unit of analysis of our study was the individual patient. The starting point for time to biochemical failure was the date treatment ended. For subjects who did not develop biochemical failure during the study, we censored follow-up time at the date of last serum PSA level assessment. First, we fitted a model by using only the Kattan linear prediction and calculated predicted treatment failure probabilities. The linear predictor is a single weighted value that combines the information of all predictor variables in a model, where the weight of each value is its association with the outcome. Next, we built a new model in which, in addition to the Kattan data, we added MR imaging variables (number of sextants with visible tumor on MR images, extracapsular extension in millimeters, presence or absence of seminal vesicle invasion, and number of sextants demonstrating malignant voxels on MR spectroscopic images) to determine the incremental prognostic value of imaging beyond the established clinical risk indicators. All imaging parameters were determined a priori. The models that included imaging variables were fitted by using the adjudicated readings. The discrimination performance of all models was determined by using receiver operating characteristic (ROC) curve analyses. We compared the areas under the ROC curve by using the algorithm suggested by DeLong et al (41).

Our sample contained complete covariate data in 57% of the subjects (n = 56). Radiation dose was the variable with most missing values (n = 25); however, it was also the variable with the least variation in the full data set. Under the assumption that data were missing at random (42), we used multiple imputation to address missing values. We used Imputation by Chained Equations in statistical software (Stata; StataCorp, College Station, Tex) to perform the 20 imputations (43). Cox models were fit by using the multiply imputed module for imputed data sets of the software (44).

Statistical calculations were performed by using statistical software (Stata, version 11; StataCorp). An α level of 5% was used for statistical significance.

We used net risk reclassification (45) to assess the added predictive value of imaging information beyond the predictors of the Kattan nomogram. With this method, the probabilities of treatment failure derived from the Kattan nomogram are compared with those obtained after combining them with MR imaging findings. More specifically, it calculates the proportion of men reclassified correctly (patients who developed biochemical failure reassigned to a higher risk category and patients who did not develop biochemical failure reassigned to a lower risk category) and that of patients reclassified incorrectly after the addition of MR imaging. To avoid the challenges of predetermining a minimum change in risk that would be considered a clinically significant difference, we opted for summarizing the net reclassification for several cut points. This factor will allow patients and physicians to opt for different cut points on the basis of individual risk-taking tolerances and perceptions about the possible outcomes of various treatments.

Results

Study Sample

Table 1 presents descriptive statistics of the study sample. The median age of our sample was 68.0 years (IQR, 59.5–72.7). Patients had a median pretreatment serum PSA level of 8.1 ng/mL (8.1 μg/L) (IQR, 5.7–14), and a median Gleason sum of 7 (IQR, 6–7). The largest percentage of patients was 38.2% for those in clinical stage T1c, followed by that of 28.9% for those in stage T2a. The percentages of patients in stages T2b, T2c, T3a, and T3b all were smaller.

Patient Treatment and Outcome

The median time between *(a)* diagnosis and MR imaging and *(b)* MR imaging and the beginning of radiation therapy was 58 days (IQR, 22–130) and 161 days (IQR, 116–213), respectively. All patients underwent a full course of definitive external-beam radiation therapy after MR imaging with a median dose of 74 Gy (IQR, 72–76). Androgen deprivation therapy was administered to 45 of 90 patients (50%). The median length of treatment was 6 months (IQR, 4–15). In nine of these patients, imaging was performed during treatment. The median follow-up time was 59.0 months (IQR, 30.7–82.1). Forty-nine men (49%) had at least 60 months of follow-up. A total of 30 patients (30%) developed biochemical failure in our study, and 16 (16%) developed biochemical failure within the first 60 months of follow-up. The median PSA level nadir was 0.5 ng/mL (0.5 μg/L) (IQR, 0.16–0.83).

MR Imaging

The two initial readers agreed on the presence or absence of cancer on MR images and on MR spectroscopic images in 69% (68 of 99) and 72% (63 of 87), respectively, of cases. In regard to the presence or absence of seminal vesicle invasion and extracapsular extension, the agreement was 95% (94 of 99) and 73% (72 of 98), respectively, of cases. In 66 cases, at least one imaging variable required adjudication.

Following adjudication, tumor was identified in 70 of 99 patients on T2-weighted MR images (71%). In patients with visible tumor, the median number of positive sextants was two (IQR, 1–3). Thirty-five of 99 patients (35%) also had findings consistent with extracapsular extension, with a mean diameter of tumor beyond the capsule of 3.5 mm (standard deviation [SD] = 2.8). Ten of 99 patients had imaging findings

Table 1

Distribution of Age and Variables That Are Inputs to the Kattan Nomogram in the Study Population and Imputed Data Set

Clinical Data	Complete Data Set: Estimates	Complete Data Set: No. of Patients	Imputed Data Set (n = 1980)
Age*	68.0 (59.5–72.7)	99	68.0
Pretreatment PSA (ng/mL)†	8.1 (5.7–14)	97	8.1
Clinical stage‡			
T1c	38	29	38.0
T2a	29	22	28.7
T2b	8	6	7.6
T2c	5	4	5.5
T3a	16	12	16.4
T3b	4	3	3.8
Gleason sum*	7 (6–7)	99	7
Gleason score§			
2 + 3	3	3	. . .
3 + 2	2	2	. . .
3 + 3	43	41	. . .
3 + 4	28	27	. . .
4 + 3	14	13	. . .
4 + 4	7	7	. . .
4 + 5	2	2	. . .
Radiation dose (Gy)*	74 (72–76)	74	74
Androgen deprivation therapy‡	51.1	45	51.1

* Data are medians, and numbers in parentheses are interquartile ranges (IQRs), except where otherwise specified.

† Data are medians, and numbers in parentheses are IQRs, except where otherwise specified. To convert PSA levels to Système International units in micrograms per liter, multiply by 1.0.

‡ Data are percentages, except where otherwise specified.

§ Data are percentages, except where otherwise specified. Percentages were rounded. Only the Gleason sum was imputed, as the Kattan nomogram uses the Gleason sum rather than Gleason scores as an input variable. Gleason scores are provided solely to describe the study population.

Figure 4

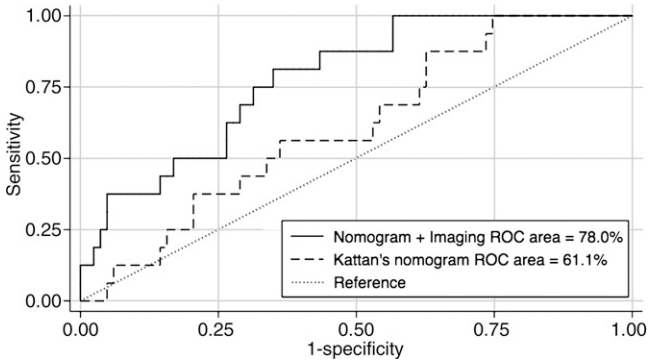

Figure 4: ROC curves for prediction of biochemical failure by using the Kattan nomogram and the nomogram combined with MR imaging findings of the prostate, with reference line.

consistent with seminal vesicle invasion (10%). Malignant metabolism on MR spectroscopic images was detected in 55 of 99 patients (56%); the median number of positive sextants was two (IQR, 2–3).

Outcome Prediction

For the Kattan nomogram, the area under the ROC curve was 61.1% (95% confidence interval: 58.1, 64.0) (Fig 4). The mean predicted 5-year probability of failure for patients who did and did not develop biochemical failure was 21.7% (SD, 4.3%) and 20.2% (SD, 5.6%), respectively.

The Cox proportional hazard model that incorporated the Kattan linear prediction and imaging findings (number of sextants with visible tumor on MR images, extracapsular extension in millimeters, presence or absence of seminal vesicle invasion, number of sextants demonstrating malignant voxels on MR spectroscopic images) showed that the extent of extracapsular extension was an independent predictor of biochemical failure at 5 years. Extracapsular extension was the only variable to be a significant predictor of treatment response (hazard ratio, 1.24; 95% confidence interval: 1.04, 1.49; P = .02).

For the model that included imaging findings, the area under the ROC curve was 78.0% (95% confidence interval: 75.7, 80.4) (Fig 4). The mean predicted 5-year probability of failure for patients who did and did not develop biochemical failure was 52.4% (SD, 24.8%) and 31.7% (SD, 16.4%), respectively.

The area under the ROC curve that is based on the model that incorporated imaging findings, as well as the Kattan linear prediction, was significantly greater than the area under the ROC curve that is based on the model with only the Kattan nomogram ($P < .001$).

Net Risk Reclassification

Overall, the addition of imaging findings led to a net improvement in risk classification (ie, percentage of correct reclassifications minus percentage of incorrect reclassifications) of roughly 28%, ranging from approximately a minimum of 16% to a maximum of 39%, depending on the risk change one considers meaningful for decision making. Table 2 summarizes the actual percentages of patients whose risk increased and did or did not develop biochemical failure; in none of the patients in our sample did the predicted risk decrease

following the addition of imaging data. Figure 5 shows a comparison of the probabilities of treatment failure determined with the use of the Kattan nomogram alone and with the use of the nomogram with MR imaging data added.

Discussion

MR imaging and MR spectroscopic imaging have been used to evaluate patients with prostate cancer and for treatment planning. Researchers in some studies have investigated the use of these techniques for prediction of patients' outcome following radiation therapy (27–29,31,46). The results of these studies have suggested that imaging findings can be used to predict treatment response. We added to this research by determining the incremental value of adding information from MR imaging to the Kattan nomogram, which is readily available for clinicians.

An improvement in our ability to predict patients' outcomes is crucial to allow men with prostate cancer to make adequate and informed decisions in regard to treatment options. For example, androgen deprivation therapy is often recommended owing to the possibility of micrometastases at the time of local treatment. If the risk of biochemical failure, which can be caused by these metastases, is determined to be minimal with external-beam radiation therapy alone, one may opt to forgo hormonal therapy. Alternatively, if the risk of failure diminishes by adding androgen deprivation therapy to the equation, one may opt to use it, despite its side effects.

In our study sample, the incorporation of imaging findings to the Kattan nomogram resulted in improved prediction of treatment failure, with an estimated net benefit occurring in 16%–39% of patients. However, the addition of MR imaging findings to the Kattan nomogram led to an increase in the predicted risk of failure for both patients who did and did not develop biochemical failure. Although improving the risk assessment of patients who indeed fail treatment is desirable, a higher predicted risk of treatment failure for men who had a good response to therapy may have clinically important implications. These patients may be subject to more aggressive or additional unnecessary therapy and its associated morbidities and costs. Similarly, MR imaging findings did not improve detection of patients in whom therapy did not fail, another desired result.

Other authors have investigated the use of MR imaging to predict response to treatment of prostate cancer. Four studies focused on radical prostatectomy (29,47–49) and four focused on radiation therapy (27,28,30,31). These latter four studies demonstrated that MR imaging findings, more specifically the amount of extracapsular extension, the presence of seminal vesicle invasion, and the volume of metabolic abnormality at MR spectroscopy, are independent predictors of treatment failure after radiation therapy. Yet, none could be used to quantify the actual benefit in terms of number of patients who gain from this prediction. In addition, in these studies, multivariate models were fitted that included various clinical, pathologic, and imaging data as independent variables,

Table 2

Net Risk Reclassification on Basis of Various Risk Changes (Threshold Levels) One May Consider Meaningful for Decision Making

	Predicted Risk Increased*		
Threshold Level (%)	With Biochemical Failure	Without Biochemical Failure	Net Risk Reclassification (%)†
10	81	42	39
20	50	23	27
30	44	13	31
40	31	5	26
50	19	2	16

* Data are percentages of patients whose risk increased after addition of MR imaging data, according to outcome. Percentages were rounded.

† Net risk reclassification was determined by subtracting the percentage of incorrect reclassifications from the percentage of correct reclassifications. Percentages were rounded.

Figure 5

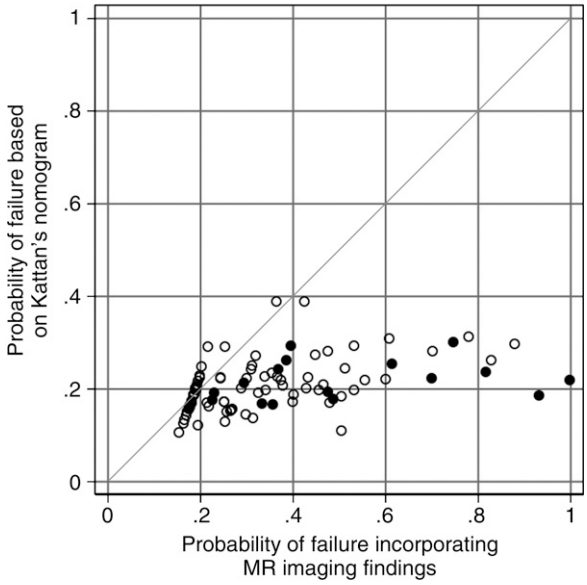

Figure 5: Net risk reclassification of predicted probabilities of treatment failure made by using the Kattan nomogram and the nomogram combined with MR imaging findings. ● = Patients who developed biochemical failure, ○ = patients who did not develop biochemical failure.

effectively laying the ground for the creation of new prediction tools. The Kattan nomogram, however, is well known and widely used in the community. By choosing to fit models on the basis of the linear predictions of the original nomogram, we were able to determine the potential value of adding MR imaging findings to a validated instrument.

Three of the studies in which researchers investigated the use of imaging in the population of men treated with radical prostatectomy also found that MR imaging findings improved prediction of treatment failure, particularly for patients with intermediate risk of recurrence that is based on clinical variables and in whom extracapsular extension and/or seminal vesicle invasion is identified (29,48,49). In the study by Fuchsjager et al (47), however, the investigators found that MR imaging findings did not provide added prognostic value to standard clinical nomograms.

Intriguingly, the performance of the Kattan nomogram in our sample was worse than expected. In the study published by Zelefsky et al (6), the C-index for the nomogram was 0.72, while in our study the area under the ROC curve was only 61%. The reason for this is unclear, but one possible explanation is that our population is different, perhaps representing a narrower range of the spectrum of disease aggressiveness when compared with the populations in which the nomogram was developed and validated. Yet, this would probably not have a substantial effect on the relative value of adding MR imaging findings to the nomogram (ie, the magnitude of the difference between ROC curves would probably not change substantially, as both models included the predictions made with the Kattan nomogram).

In concordance with data in prior studies (27,29,31), we found that extracapsular extension was an independent predictor of treatment failure, but seminal vesicle invasion was not predictive of treatment response (28–30). This was a surprising finding, as seminal vesicle invasion is widely believed to be associated with larger tumors with a poorer prognosis; our study is small and may have been underpowered to demonstrate the importance of this variable. In our sample, prediction of biochemical failure related to imaging findings was mostly driven by the amount of extracapsular extension, as it was the only independent predictor.

In addition, MR imaging may have other important roles in treatment planning. Davis et al (50), for instance, have shown that the diameter of extracapsular extension influences radiation treatment planning, because the dose decline at the periphery of the field may result in incomplete treatment. Neither of these was considered in our work, and further research is required to confirm these hypotheses.

Some may argue that mortality would be a preferable outcome to measure. However, because of the long time required to measure this outcome, we opted for using biochemical failure. Biochemical failure is a widely used and accepted surrogate (40), and, although it does not always represent local recurrence or metastatic disease, Kwan et al (51) showed that it was associated with worse survival, particularly in younger patients with high-risk disease.

While some may consider missing data a weakness of the study, we used well-known validated techniques to deal with the problem. It is important to note that following imputation, the measurements of central tendency and dispersion did not change significantly (Table 1); that is, the complete and imputed data sets look alike and the use of imputation mostly increased statistical power.

Our study had limitations. First, because of its retrospective nature, the time among diagnosis, imaging acquisition, and start of external-beam radiation therapy was not predetermined. Because of the variation, it is conceivable that some of the prostate cancers may have grown during these intervals. If this happened, in our study we could have overestimated the value of pretreatment MR imaging. Second, similarly, in nine of 45 patients who were treated with androgen deprivation therapy, MR images were obtained during hormonal treatment. It is possible that some of the tumors were less conspicuous on images and their extension throughout the gland could have been underestimated with T2-weighted MR imaging and MR spectroscopic imaging. If this were the case, our results would lead to underestimation of the incremental benefit of imaging. Third, this was a single-institution study; therefore, our results may not be generalizable, owing to differences in imaging acquisition and expertise in imaging interpretation among various institutions. Fourth, the heterogeneity of our population and treatment protocols influenced our imaging results; however, the prediction made by using the nomogram was also affected. Fifth, MR imaging has been shown to be more accurate than digital rectal examination for localizing disease within the prostate (24), and one could argue that the assessment of clinical stage made by the clinician could have been biased on the basis of MR results. If this occurred, the bias would be in favor of the Kattan nomogram. To minimize this problem, care was taken to register the description of clinical stage in notes dated prior to MR imaging. Finally, our study sample was small, and we were not able to perform cross-validation (internal validation using a subset of our own sample). A larger, preferably prospective, study is needed to validate our results and develop a new nomogram that incorporates imaging findings and that can be used in everyday practice.

In summary, MR imaging data improve the prediction of biochemical failure with the Kattan nomogram after external-beam radiation therapy for prostate cancer; this is mostly related to the amount of extracapsular extension seen on images. Accordingly, the net risk improvement was due to better prediction of treatment failures rather than to identification of patients who respond well to treatment. The number needed to image to improve the prediction of biochemical failure in one patient ranges from three to six.

Acknowledgments: The authors thank Michael W. Kattan, MBA, PhD, for sharing his research data, and Amy J. Markowitz, JD, consulting editor and scientific writing specialist, for her help in editing the manuscript.

Disclosures of Potential Conflicts of Interest: A.C.W. No potential conflicts of interest to disclose. **W.J.K.** No potential conflicts of interest to disclose. **F.V.C.** No potential conflicts of interest to disclose. **V.F.M.** No potential conflicts of interest to disclose. **J.M.N.** No potential conflicts of interest to disclose. **R.T.M.** No potential conflicts of interest to disclose. **J.K.** No potential conflicts of interest to disclose. **R.S.** No potential conflicts of interest to disclose.

References

1. Kestin LL, Vicini FA, Ziaja EL, Stromberg JS, Frazier RC, Martinez AA. Defining biochemical cure for prostate carcinoma patients treated with external beam radiation therapy. Cancer 1999;86(8):1557–1566.
2. Moul JW. Prostate specific antigen only progression of prostate cancer. J Urol 2000; 163(6):1632–1642.
3. Stephenson RA, Stanford JL. Population-based prostate cancer trends in the United States: patterns of change in the era of prostate-specific antigen. World J Urol 1997; 15(6):331–335.
4. Chun FK, Karakiewicz PI, Briganti A, et al. Prostate cancer nomograms: an update. Eur Urol 2006;50(5):914–926; discussion 926.
5. Kattan MW, Zelefsky MJ, Kupelian PA, Scardino PT, Fuks Z, Leibel SA. Pretreatment nomogram for predicting the outcome of three-dimensional conformal radiotherapy in prostate cancer. J Clin Oncol 2000;18(19): 3352–3359.
6. Zelefsky MJ, Kattan MW, Fearn P, et al. Pretreatment nomogram predicting ten-year biochemical outcome of three-dimensional conformal radiotherapy and intensity-modulated radiotherapy for prostate cancer. Urology 2007;70(2):283–287.
7. Bolla M, Collette L, Blank L, et al. Long-term results with immediate androgen suppression and external irradiation in patients with locally advanced prostate cancer (an EORTC study): a phase III randomised trial. Lancet 2002;360(9327):103–106.
8. Roach M 3rd, Bae K, Speight J, et al. Short-term neoadjuvant androgen deprivation therapy and external-beam radiotherapy for locally advanced prostate cancer: long-term results of RTOG 8610. J Clin Oncol 2008; 26(4):585–591.
9. Roehl KA, Antenor JA, Catalona WJ. Serial biopsy results in prostate cancer screening study. J Urol 2002;167(6):2435–2439.
10. Stewart CS, Leibovich BC, Weaver AL, Lieber MM. Prostate cancer diagnosis using a saturation needle biopsy technique after previous negative sextant biopsies. J Urol 2001;166(1):86–91; discussion 91–92.
11. Fleshner N, Klotz L. Role of "saturation biopsy" in the detection of prostate cancer among difficult diagnostic cases. Urology 2002;60(1):93–97.
12. Bauer JJ, Zeng J, Zhang W, et al. 3-D computer visualization and interactive prostate biopsy simulation leads to an improved systematic technique for the detection of prostate cancer: clinical correlation. Stud Health Technol Inform 2000;70:20–25.
13. Tavangar SM, Razi A, Mashayekhi R. Correlation between prostate needle biopsy and radical prostatectomy Gleason gradings of 111 cases with prostatic adenocarcinoma. Urol J 2004;1(4):246–249.
14. Hostetter AL, Pedersen KV, Gustafsson BL, Månson JC, Boeryd BR. Diagnosis and localization of prostate carcinoma by fine-needle aspiration cytology and correlation with histologic whole-organ sections after radical prostatectomy. Am J Clin Pathol 1990; 94(6):693–697.
15. Mazzucchelli R, Colanzi P, Pomante R, Muzzonigro G, Montironi R. Prostate tissue and serum markers. Adv Clin Path 2000; 4(3):111–120.
16. Kuban DA, Thames HD, Levy LB, et al. Long-term multi-institutional analysis of stage T1-T2 prostate cancer treated with radiotherapy in the PSA era. Int J Radiat Oncol Biol Phys 2003;57(4):915–928.
17. D'Amico AV, Whittington R, Malkowicz SB, et al. Pretreatment nomogram for prostate-specific antigen recurrence after radical prostatectomy or external-beam radiation therapy for clinically localized prostate cancer. J Clin Oncol 1999;17(1):168–172.
18. Katz S, Rosen M. MR imaging and MR spectroscopy in prostate cancer management. Radiol Clin North Am 2006;44(5):723–734.
19. Rajesh A, Coakley FV. MR imaging and MR spectroscopic imaging of prostate cancer. Magn Reson Imaging Clin N Am 2004; 12(3):557–579.
20. Rajesh A, Coakley FV, Kurhanewicz J. 3D MR spectroscopic imaging in the evaluation of prostate cancer. Clin Radiol 2007; 62(10):921–929.
21. Casciani E, Polettini E, Bertini L, et al. Prostate cancer: evaluation with endorectal MR imaging and three-dimensional proton MR spectroscopic imaging. Radiol Med (Torino) 2004;108(5-6):530–541.
22. Casciani E, Polettini E, Bertini L, et al. Contribution of the MR spectroscopic imaging in the diagnosis of prostate cancer in the peripheral zone. Abdom Imaging 2007;32(6): 796–802.
23. Fütterer JJ, Heijmink SW, Scheenen TW, et al. Prostate cancer localization with dynamic contrast-enhanced MR imaging and proton MR spectroscopic imaging. Radiology 2006;241(2):449–458.
24. Mullerad M, Hricak H, Kuroiwa K, et al. Comparison of endorectal magnetic resonance imaging, guided prostate biopsy and digital rectal examination in the preoperative anatomical localization of prostate cancer. J Urol 2005;174(6):2158–2163.
25. Pucar D, Shukla-Dave A, Hricak H, et al. Prostate cancer: correlation of MR imaging and MR spectroscopy with pathologic findings after radiation therapy-initial experience. Radiology 2005;236(2):545–553.
26. Santos CF, Kurhanewicz J, Tabatabai ZL, et al. Metabolic, pathologic, and genetic analysis of prostate tissues: quantitative evaluation of histopathologic and mRNA integrity after HR-MAS spectroscopy. NMR Biomed 2010;23(4):391–398.
27. McKenna DA, Coakley FV, Westphalen AC, et al. Prostate cancer: role of pretreatment MR in predicting outcome after external-beam radiation therapy—initial experience. Radiology 2008;247(1):141–146.
28. Joseph T, McKenna DA, Westphalen AC, et al. Pretreatment endorectal magnetic resonance imaging and magnetic resonance spectroscopic imaging features of prostate cancer as predictors of response to external beam radiotherapy. Int J Radiat Oncol Biol Phys 2009;73(3):665–671.
29. Cheng GC, Chen MH, Whittington R, et al. Clinical utility of endorectal MRI in determining PSA outcome for patients with biopsy Gleason score 7, PSA <or=10, and clinically localized prostate cancer. Int J Radiat Oncol Biol Phys 2003;55(1):64–70.
30. Nguyen PL, Whittington R, Koo S, et al. Quantifying the impact of seminal vesicle invasion identified using endorectal magnetic resonance imaging on PSA outcome after radiation therapy for patients with clinically localized prostate cancer. Int J Radiat Oncol Biol Phys 2004;59(2):400–405.
31. Fuchsjäger MH, Pucar D, Zelefsky MJ, et al. Predicting post-external beam radiation therapy PSA relapse of prostate cancer using pretreatment MRI. Int J Radiat Oncol Biol Phys 2010;78(3):743–750.
32. Wang L, Hricak H, Kattan MW, et al. Prediction of seminal vesicle invasion in prostate cancer: incremental value of adding endorectal MR imaging to the Kattan nomogram. Radiology 2007;242(1):182–188.
33. Wang L, Hricak H, Kattan MW, Chen HN, Scardino PT, Kuroiwa K. Prediction of organ-confined prostate cancer: incremental value of MR imaging and MR spectroscopic imaging to staging nomograms. Radiology 2006; 238(2):597–603.

34. Schricker AA, Pauly JM, Kurhanewicz J, Swanson MG, Vigneron DB. Dualband spectral-spatial RF pulses for prostate MR spectroscopic imaging. Magn Reson Med 2001;46(6):1079–1087.

35. Star-Lack J, Vigneron DB, Pauly J, Kurhanewicz J, Nelson SJ. Improved solvent suppression and increased spatial excitation bandwidths for three-dimensional PRESS CSI using phase-compensating spectral/spatial spin-echo pulses. J Magn Reson Imaging 1997;7(4):745–757.

36. Tran TK, Vigneron DB, Sailasuta N, et al. Very selective suppression pulses for clinical MRSI studies of brain and prostate cancer. Magn Reson Med 2000;43(1):23–33.

37. Sala E, Akin O, Moskowitz CS, et al. Endorectal MR imaging in the evaluation of seminal vesicle invasion: diagnostic accuracy and multivariate feature analysis. Radiology 2006;238(3):929–937.

38. Jung JA, Coakley FV, Vigneron DB, et al. Prostate depiction at endorectal MR spectroscopic imaging: investigation of a standardized evaluation system. Radiology 2004; 233(3):701–708.

39. Abramowitz MC, Li T, Buyyounouski MK, et al. The Phoenix definition of biochemical failure predicts for overall survival in patients with prostate cancer. Cancer 2008; 112(1):55–60.

40. Roach M 3rd, Hanks G, Thames H Jr, et al. Defining biochemical failure following radiotherapy with or without hormonal therapy in men with clinically localized prostate cancer: recommendations of the RTOG-ASTRO Phoenix Consensus Conference. Int J Radiat Oncol Biol Phys 2006;65(4):965–974.

41. DeLong ER, DeLong DM, Clarke-Pearson DL. Comparing the areas under two or more correlated receiver operating characteristic curves: a nonparametric approach. Biometrics 1988;44(3):837–845.

42. Schafer JL. Multiple imputation: a primer. Stat Methods Med Res 1999;8(1):3–15.

43. Patrick R. ICE: Stata module for multiple imputation of missing values. S446602 ed. Boston, Mass: Boston College Department of Economics, 2006.

44. Galati JS, Royston P, Carlin JB. MIM: Stata module to analyse and manipulate multiply imputed datasets. Statistical Software Components. Boston, Mass: Boston College Department of Economics, 2007.

45. Pencina MJ, D'Agostino RB Sr, D'Agostino RB Jr, Vasan RS. Evaluating the added predictive ability of a new marker: from area under the ROC curve to reclassification and beyond. Stat Med 2008;27(2):157–172; discussion 207–212.

46. D'Amico AV, Halabi S, Tempany C, et al. Tumor volume changes on 1.5 tesla endorectal MRI during neoadjuvant androgen suppression therapy for higher-risk prostate cancer and recurrence in men treated using radiation therapy results of the phase II CALGB 9682 study. Int J Radiat Oncol Biol Phys 2008;71(1):9–15.

47. Fuchsjäger MH, Shukla-Dave A, Hricak H, et al. Magnetic resonance imaging in the prediction of biochemical recurrence of prostate cancer after radical prostatectomy. BJU Int 2009;104(3):315–320.

48. Poulakis V, Witzsch U, de Vries R, et al. Preoperative neural network using combined magnetic resonance imaging variables, prostate specific antigen, and Gleason score to predict prostate cancer recurrence after radical prostatectomy. Eur Urol 2004;46(5):571–578.

49. D'Amico AV, Whittington R, Malkowicz B, et al. Endorectal magnetic resonance imaging as a predictor of biochemical outcome after radical prostatectomy in men with clinically localized prostate cancer. J Urol 2000; 164(3 pt 1):759–763.

50. Davis BJ, Pisansky TM, Wilson TM, et al. The radial distance of extraprostatic extension of prostate carcinoma: implications for prostate brachytherapy. Cancer 1999;85(12): 2630–2637.

51. Kwan W, Pickles T, Duncan G, et al. PSA failure and the risk of death in prostate cancer patients treated with radiotherapy. Int J Radiat Oncol Biol Phys 2004;60(4):1040–1046.